# Electromagnetic Induction Based Regional Subsurface Characterization of Mountainous Environments: Examples from Puerto Rico

**Parker S. Blunts,[1] Dimitrios Zekkos, Ph.D., P.E., M. ASCE[2], and Marin Clark, Ph.D.[3]**

[1]Dept. of Civil and Environmental Engineering, University of California Berkeley, Berkeley, CA. E-mail: parkerj@berkeley.edu
[2]Dept. of Civil and Environmental Engineering, University of California Berkeley, Berkeley, CA. E-mail: zekkos@berkeley.edu
[3]Dept. of Earth and Environmental Sciences, University of Michigan, Ann Arbor, MI. E-mail: marinkc@umich.edu

## ABSTRACT

The physical and mechanical characterization of the subsurface under hillslopes is critical for understanding the distribution of mass wasting by landslides and debris flows, which are two significant processes that drive topographic change in steep environments. Hillslope environments are notoriously spatially complex. However, subsurface characterization is rarely performed on regional scales due to challenges in characterizing highly localized variations. Common methods for subsurface characterization involve costly site-specific sampling and testing leading to point measurements or regional remote sensing techniques. Currently, a gap in scale compatibility exists between site-specific analysis where characterization of the subsurface is robust but spatially limited and regional hazard analyses where characterization is limited to regionally broad categories based on lithology, slope, and/or vegetation. This research explores electromagnetic induction (EM) as a scalable approach to characterize relative differences in physico-mechanical properties of the subsurface in steep terrain where mass wasting is common. For this study, EM data was collected in different geologic units across southwest Puerto Rico (PR), then converted to apparent resistivity values. The apparent resistivity of lithologic groups and limestone subunits were statistically compared leveraging the large datasets collected. Two study areas are selected to examine spatial trends and the effects of topographic factors. The results indicate that EM can detect differences between and within geologic units/subunits and help estimate subsurface heterogeneity where detailed mapping is unavailable.

## INTRODUCTION

As the global population continues to grow, increasing urbanization and population density exposes more people to natural hazards such as hurricanes, earthquakes, and landslides (Donner and Rodriguez 2008). Puerto Rico is a Caribbean Island and United States territory located approximately 1,600 km from the coast of Florida that experiences many of these hazards. In 2017, Hurricane Maria caused tens of thousands of landslides which significantly damaged infrastructure and killed 64 people (Silva-Tulla et al. 2018, Morales et al. 2022). The 2019-2020 earthquake sequence caused two deaths and at least 800 landslides in a variety of geologic units (Morales-Velez et al. 2020). In 2022, Hurricane Fiona killed one person, severely damaged infrastructure, and caused thousands of landslides (Morales et al. 2022). Landslides in these three events ranged from shallow debris flows and rockfall to deep seated landslides, with some geologic units experiencing much higher landslide concentrations than others (Silva-Tulla et al.

2018, Morales-Velez et al. 2020, Morales et al. 2022). Characterizing variation within and between geologic units and subunits is critical for understanding the spatial distribution of landsliding as well as for landslide modeling and hazard prediction. However, scalable approaches that can be used to characterize large areas are lacking. In this study, EM is used as a scalable geophysical method for subsurface characterization of large areas.

EM is a geophysical method used to detect spatial differences in conductive materials of the subsurface without direct contact (Doolittle and Brevik 2014, Finco et al. 2023). Given EM is a rapid, non-invasive, and non-contact method, it can be a cost-effective technique to survey larger areas compared to other geophysical methods such as seismic geophysics or direct contact electrical resistivity tomography (Doolittle and Brevik 2014, Finco et al. 2023). EM uses an electrical current run through a transmission coil at preset frequencies to create a magnetic field. This primary magnetic field then induces eddy currents in conductive materials within the subsurface. The eddy currents create a secondary magnetic field which is measured in a secondary receiver coil at the surface. Both the primary and secondary magnetic fields are received at the receiving coil so some devices (including the one used in this study) have a third "bucking" coil to remove the signal of the primary field (Won et al. 1996, Finco et al. 2023). The relative change of impedance between the two coils in parts per million (PPM) is the raw signal of EM. The difference in phase and amplitude provides information on the subsurface (Won et al. 1996, Allred et al. 2008, Finco et al. 2023). The depth of investigation for EM is dependent on the subsurface conditions, the frequency of transmitted signal, and separation between the transmitting and receiving coil (Won et al. 1996, Huang 2005, Allred et al. 2008).

EM is sensitive to factors that affect electrical conductivity such as moisture, clay content, mineralogy, soil texture, salinity, organics, gradation, density, weathering, induration, and silification (Allred et al. 2008, Doolittle and Brevik 2014, Hubbard et al. 2021, Mohammed 2022). EM has been used in the mining industry for mineral prospecting (Smith 2013) and for soil studies to map clay content such as Triantafilis and Lesch (2005). Other studies such as Hubbard et al. (2021) used EM to map soil classes for wine vineyards and Mohammed et al. (2022) used EM to look at soil texture and salinity. However, most of these studies use near surface EM with a focus on environmental, ecological, petrological, and hydrological applications. In geotechnical applications, Godio and Bottino (2001) and McCann and Forster (1990) used EM for site-specific landslide characterization, recognizing its value in identifying landslide geometry, hydrogeological regime, and clay content, but did not apply the method at large scales. A gap in existing literature exists between using EM for site-specific and regional applications. Although handheld electromagnetic devices are commonly employed in environmental applications, the field of geologic mapping predominantly utilizes airborne EM. In this paper, we present an innovative application of handheld EM technology as a versatile multiscale geotechnical assessment tool for discerning variability in subsurface properties. This novel methodology entails the application of a well-established approach, harnessing handheld EM instruments across varying scales. This expansion broadens its potential utilization and amalgamates prior applications, thereby enhancing its efficacy within the realm of geotechnical analysis.

## DATA AND METHODS

**Data Collection.** EM data was collected using a GEM2 frequency domain electromagnetic sensor (FDEM) produced by Geophex Ltd. that utilizes continuous energy

transmission of multiple frequencies simultaneously (Won et al. 1996). The device has a fixed spacing of 1.66m and was operated at a target height between 0.92 m and 1.0 m with minor variations due to surface conditions. The frequencies used were 450 Hz, 1530 Hz, 5310 Hz, 18330 Hz, and 63030 Hz with concurrent data collection of all frequencies. These frequencies were selected to provide a range of depths as frequency is inversely related to depth of investigation. The GEM2 sampling rate was set to 10 Hz and was operated in horizontal coplanar mode. Two Emlid RS2 multi-band GPS receivers were deployed in real-time kinematic (RTK) mode to achieve precise GPS positioning for EM data acquisition.

Data collection occurred between May 26, 2022 - May 31, 2022. Approximately 156,000 EM data points were collected around the southwest quadrant of the island totaling approximately 22.5 km of survey transects (Figure 1). Data was collected in a variety of different geologic units, topographic conditions, and climatic environments.

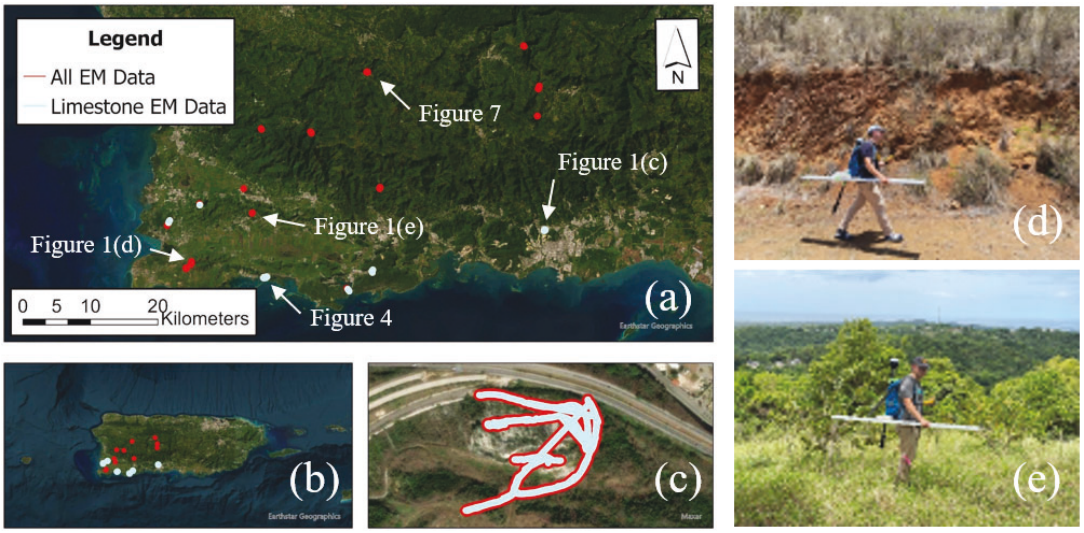


**Figure 1. Maps and pictures of data collection: (a) spatial extent of EM data collected, (b) overview map of EM data collected, (c) enlarged map of Ponce Limestone survey, (d) photo of data collection in arid region, (e) photo of data collection in humid region.**

**Processing.** EM data was processed using ArcGIS Pro for geospatial analysis and filtered using Python via Jupyter Notebooks. The raw EM signature for each frequency was converted to apparent conductivity using relationships developed by Won et al. (1996). These apparent conductivity values were converted to apparent resistivity values as conductivity and resistivity are inversely related. Apparent resistivity is a derived indirect measurement useful for spatial comparison but distinct from a material's intrinsic true resistivity. Data filtering was also conducted including removal of spatially abrupt high resistivity values through a 500 ohm-meter cutoff that was considered indicative of non-geologic subsurface features. Different lithologies were also considered using a United States Geologic Survey map (Bawiec 1998). Data in eight mapped limestone subunits was identified for comparison. These groups and subunits can be found in Table 1 and Table 2 respectively.

## RESULTS AND DISCUSSION

**Lithologic Units and Subunits**. The statistical median and distribution of apparent resistivities may potentially distinguish (sub) units of differing mineralogy, grain size, and

weathering degree. Here we show the medians and standard deviations of apparent resistivities for the mapped lithologic groups (Bawiec 2018) are shown in Table 1 for all frequencies used. In addition, Figure 2 illustrates box plots representing quantiles for the 63030 Hz frequency, which is the highest frequency used in the study. To mitigate outlier effects from anthropogenic sources, the median (as opposed to mean) was chosen for comparison. The metamorphic and plutonic batholith groups have higher median values and higher standard deviations while the alluvium group has lower median values and higher standard deviations compared to the other groups (Table 1 and Figure 2). The greater range in the alluvium data is not surprising given the expected variability of that unit. The other five groups have intermediate median values with different standard deviations. Similar trends are also observed for the remaining EM frequencies as shown in Table 1. Note that the standard deviations get progressively higher at lower frequencies indicating a lower signal to noise ratio with decreasing frequency and increasing depth. Nevertheless, the results indicate that there are differences between the various lithologic units that can be observed in the EM data.

**Table 1. Lithologic groupings for comparison based on mapped geologic units.**

| Group | Data Points in Raw Data | Data Points in Filtered Data | Percentage of Data Points Removed | Resistivity [Ohm-m] 63030 Median | Resistivity [Ohm-m] 63030 Std Dev | Resistivity [Ohm-m] 18330 Median | Resistivity [Ohm-m] 18330 Std Dev | Resistivity [Ohm-m] 5310 Median | Resistivity [Ohm-m] 5310 Std Dev | Resistivity [Ohm-m] 1530 Median | Resistivity [Ohm-m] 1530 Std Dev | Resistivity [Ohm-m] 450 Median | Resistivity [Ohm-m] 450 Std Dev |
|---|---|---|---|---|---|---|---|---|---|---|---|---|---|
| Alluvium | 10417 | 9225 | 11.4 | 6.5 | 25.4 | 6.3 | 39.6 | 5.7 | 65.1 | 4 | 41.4 | 1.8 | 53.2 |
| Volcanic | 14831 | 11699 | 21.1 | 32.2 | 11.1 | 36.9 | 26.4 | 40.3 | 47.2 | 20.7 | 64.5 | 4.1 | 69.3 |
| Metamorphic | 10611 | 9088 | 14.4 | 47.9 | 19.7 | 58 | 34 | 57.6 | 71.6 | 19.4 | 54.9 | 4.2 | 55.5 |
| Volcaniclastic | 41494 | 32345 | 22 | 32.1 | 14.5 | 37 | 22.9 | 37.3 | 48.8 | 20.5 | 44.6 | 4.1 | 72.8 |
| Sedimentary | 3730 | 3611 | 3.2 | 28.8 | 19.3 | 28.1 | 30.4 | 24 | 62.8 | 10.9 | 41.2 | 2.7 | 14 |
| Limestone | 56339 | 55086 | 2.2 | 25.9 | 20.3 | 24.7 | 27.2 | 21.4 | 44.4 | 10.5 | 38.1 | 3.2 | 26.3 |
| Plutonic Batholith | 23367 | 18412 | 21.2 | 47 | 18.4 | 60 | 40.7 | 59.9 | 81 | 20.1 | 73.6 | 4.2 | 56.7 |

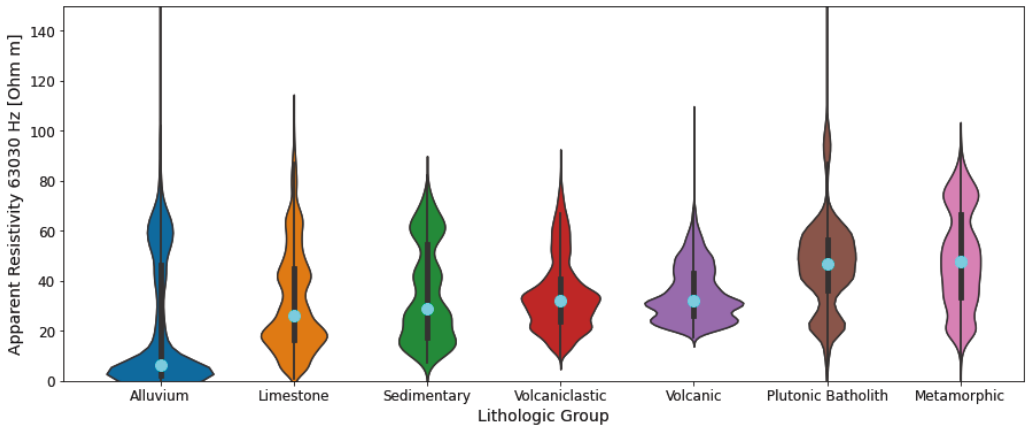


**Figure 2. Violin plots for resistivity distribution of different lithologic groups. Blue dot indicates median value.**

One of the units of particular interest in this study is the limestone unit. The limestone unit has a median value of 25.9 Ohm-meters and a standard deviation of 20.3 Ohm-meters at 63030 Hz and lower resistivities at lower frequencies. Landslides occurring during the 2019-2020 earthquake sequence were limited to the limestone units (Morales-Velez 2020), which have an intermediate variation compared to the remaining lithologic units (Table 1 and Figure 2). The limestone units consist of several subunits and analyses were conducted to observe any systematic differences in the EM signal between the subunits. The medians and standard

deviations of the limestone subunits can be seen in Table 2 and visualized with box plots representing quantiles of apparent resistivity for the 63030 Hz frequency in Figure 3. The Ponce Limestone, the Lower Member of the Parguera Limestone, and the Limestone Member of the Juana Diaz Formation have higher median values and standard deviations for apparent resistivity at the 63030 Hz frequency (Table 2 and Figure 3). The other five groups have lower median values and lower standard deviations. Similar trends are observed for the lower frequencies as shown in Table 2.

The results indicate that EM can detect systematic differences in physical properties between the various subunits that are likely correlated with mechanical properties. For example, higher resistivities are observed for units observed to be more intact and of lower porosity. The limestone units vary in geologic age where the Cotui formation is the oldest geologic unit (Mid to upper Cretaceous), followed by the Parguera formation (Upper Cretaceous) and Sabana Grande formation (Upper Cretaceous), the Juana Diaz formation (Mid Miocene) and the Ponce formation (upper Miocene) (Monroe 1980). In general, increasing resistivities are observed for the limestone sub-units with decreasing age. During the 2017 Hurricane Maria, the 2022 Hurricane Fiona, and the 2019-2020 Puerto Rico earthquake sequence, the Juana Diaz formation was found to have a much higher number of landslides than the Ponce or the Parguera formation (Silva-Tulla et al. 2018, Morales-Velez et al., 2020, Morales et al. 2022). While the median values of apparent resistivity for the Parguera, the Juana Diaz, and the Ponce were similar, the distribution of the data gives a better sense of the variability between and within these units. The Ponce has a large spread and higher resistivities while the Parguera also has a large spread but with lower quantiles. The Juana Diaz has a smaller spread and standard deviation, indicating less variability.

**Table 2. Limestone subunits used for comparison based on mapped geologic units.**

| Subunit | Data Points in Raw Data | Data Points in Filtered Data | Percentage of Data Points Removed | Resistivity [Ohm-m] 63030 Median | Resistivity [Ohm-m] 63030 Std Dev | Resistivity [Ohm-m] 18330 Median | Resistivity [Ohm-m] 18330 Std Dev | Resistivity [Ohm-m] 5310 Median | Resistivity [Ohm-m] 5310 Std Dev | Resistivity [Ohm-m] 1530 Median | Resistivity [Ohm-m] 1530 Std Dev | Resistivity [Ohm-m] 450 Median | Resistivity [Ohm-m] 450 Std Dev |
|---|---|---|---|---|---|---|---|---|---|---|---|---|---|
| Ponce Limestone | 8583 | 8337 | 2.9 | 44.2 | 22.2 | 40.2 | 36.3 | 32.5 | 55 | 13 | 56.8 | 3.5 | 15 |
| Juana Díaz Formation; Limestone member | 5723 | 5664 | 1 | 42.4 | 12.9 | 45.3 | 17.7 | 39.6 | 32.7 | 14.4 | 37.7 | 4.1 | 38.7 |
| Parguera Limestone; Lower Member | 18032 | 17581 | 2.5 | 41.4 | 21.6 | 44.9 | 28.1 | 39.1 | 58 | 13.1 | 42.1 | 3.1 | 20.7 |
| Cotuí Limestone | 5896 | 5583 | 5.3 | 22.6 | 8.2 | 24.4 | 9.8 | 26 | 15.7 | 16.2 | 38.6 | 3.7 | 40.9 |
| Sabana Grande Formation; Limestone Lenses | 930 | 808 | 13.1 | 22.1 | 5.9 | 24.3 | 6.4 | 25.2 | 6.6 | 17 | 8.2 | 5.8 | 54.5 |

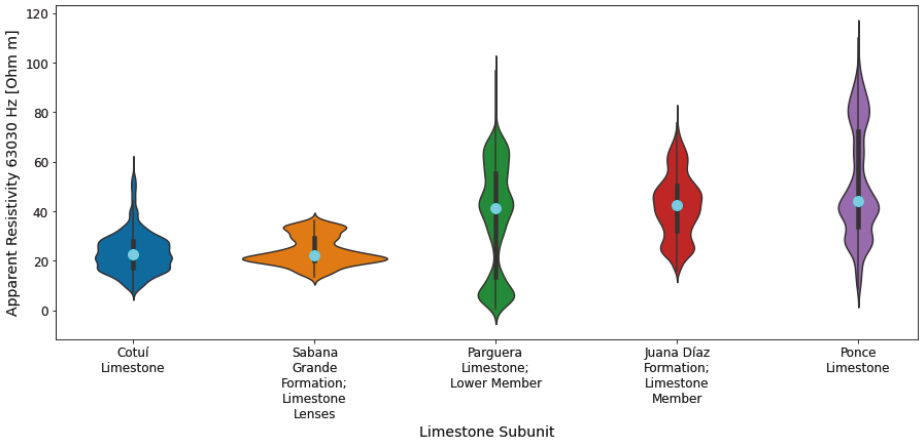

**Figure 3. Violin plots for resistivity distribution of different limestone subunits. Blue dot indicates median value.**

**Geospatial Analysis of the Parguera Limestone Data**. Spatial variability was also considered as an additional factor. One of the limestone subunits considered was the Lower Member of the Parguera Limestone. The spatial distribution of the EM data and the apparent resistivities at 63030 Hz and 5310 Hz are shown in Figure 4 on satellite imagery basemap. Systematic differences in resistivity are observed within the same geologic subunit with higher resistivities observed on the southwestern slopes compared to northeastern slopes. Although EM cannot provide a definitive reason for these differences, lower resistivities are generally associated with higher porosity (if saturated) and wetter materials. Observed trends may indicate a difference in rock structure, degree of fracturing, saturation/water content, mineralogy, clay content, porosity, or other factors.

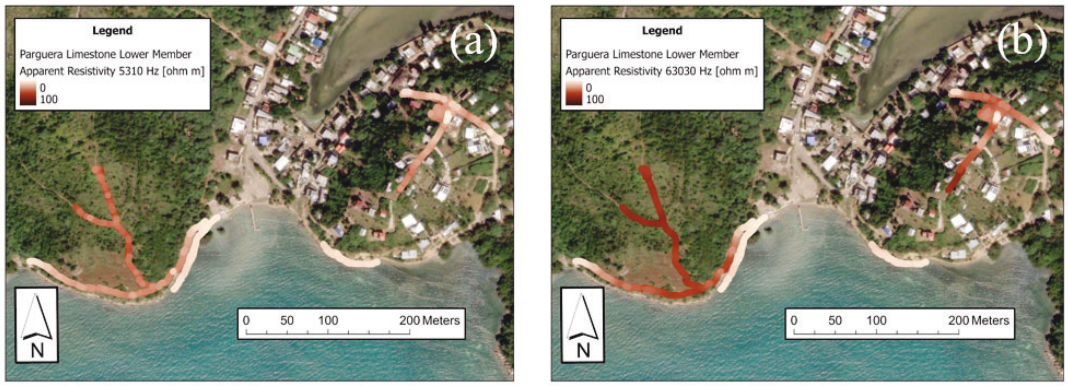


**Figure 4. Map illustrating geospatial distribution of EM data collected in the Paguera Limestone Lower Member for (a) 5310 Hz and (b) 63030 Hz.**

Additional analyses were conducted to assess the sources of spatial variability including the influence of topography. Figure 5 illustrates a stacked histogram of apparent resistivity, with coloration denoting elevation levels. For the Parguera Limestone, low elevation areas have lower resistivity as shown in Figure 5 and Figure 6. The trimodal distribution of apparent resistivity as shown in Figure 5 is attributed to the saline water of the ocean and variable water table. Areas near zero elevation are practically submerged in saline water, whereas areas at higher elevation are visibly drier.

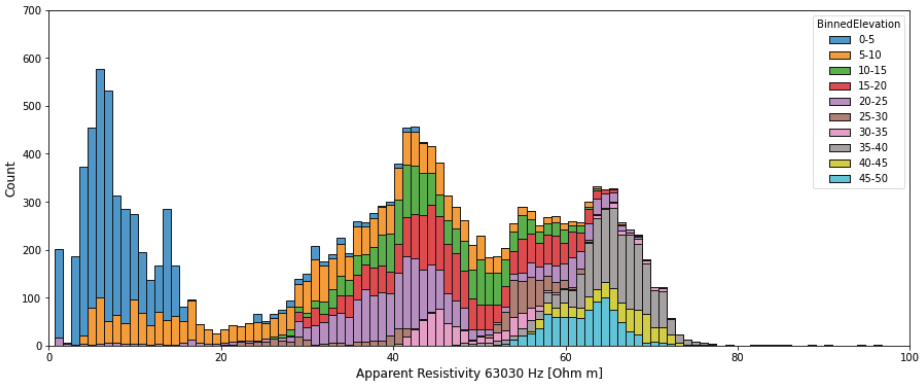

**Figure 5. Stacked histogram of apparent resistivity colored by binned elevation for 63030 Hz apparent resistivity in the Paguera Limestone.**

To quantify the relationship between elevation and apparent resistivity, ordinary least squares (OLS) multivariate regressions were performed using various topographic parameters (elevation, aspect (defined as the azimuth of a slope), slope, and geographic position) that were derived from a 1/3 arc-second resolution DEM (USGS 2020). The model regression has an R-squared of 0.847 (Figure 6). A single variable regression against elevation has an R-squared of 0.748, which is indicative of the importance of elevation, but also the influence of other parameters.

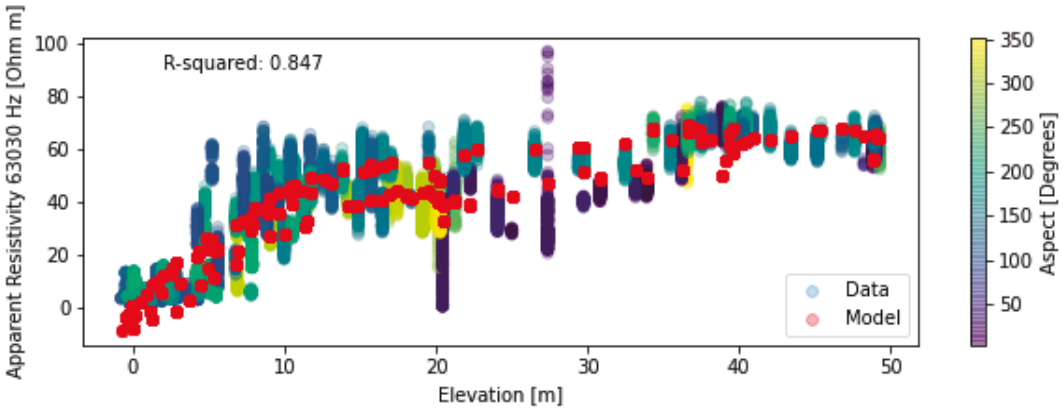


**Figure 6. Apparent resistivity for the Parguera Limestone plotted with elevation and colored by aspect with an OLS multivariate regression.**

**Geospatial Analysis of the Rio Blanco Mountain Data**. In the context of the Parguera limestone, elevation emerged as the dominant parameter, displaying the strongest correlation with the observed spatial distribution of apparent resistivity. Analysis was also conducted at the Rio Blanco Mountain, located in the predominantly breccia and tuff Milagros Formation. Figure 7 shows the EM data plotted geospatially for 63030 Hz and 18330 Hz using a 1/3 arc-second resolution DEM for the basemap (USGS 2020). As depicted in Figures 7 and 8, a discernible pattern emerges, revealing higher resistivity values in the southwestern region compared to the northeast. Geospatial and multivariate regression analysis confirms aspect as the parameter with the most substantial observed correlation.

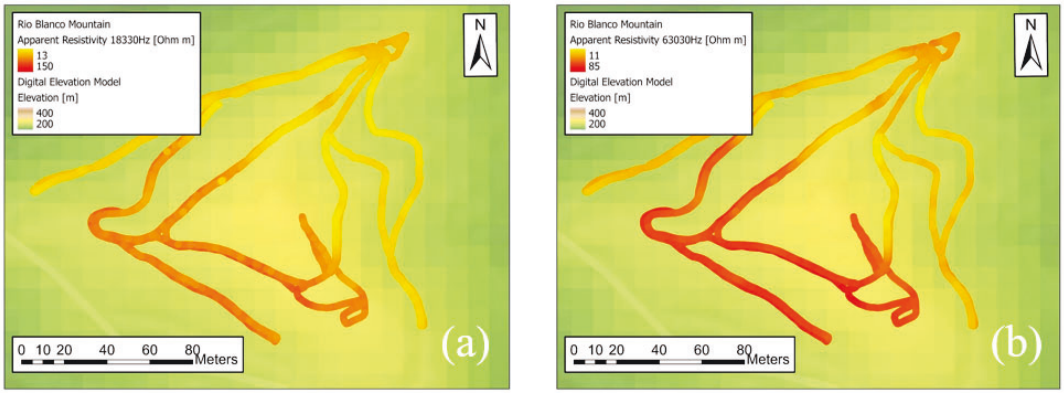

**Figure 7. Geospatial distribution of EM data collected around Rio Blanco Mountain for: (a) 18330 Hz data and (b) 63030 Hz data.**

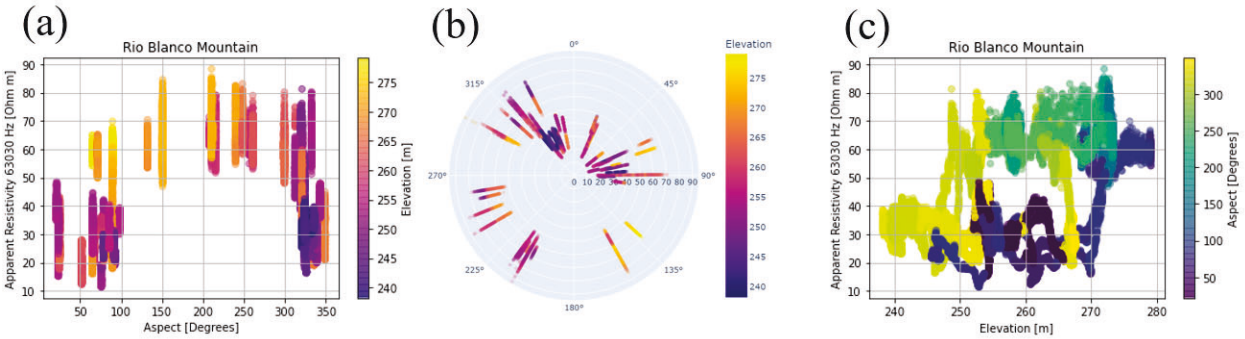


**Figure 8. Apparent resistivity related to aspect and elevation visualized on (a & c) a cartesian plot, and (b) a polar plot where distance from the origin represents apparent resistivity.**

Figure 8 presents apparent resistivity in color-coded form, emphasizing its correlations with aspect and elevation. Specifically, Figure 8c depicts apparent resistivity in relation to elevation but color-coded by aspect, revealing that aspect overwhelmingly influences the signal, potentially overshadowing any elevation-related patterns. Notably, the results unveil a distinct non-linear trend with aspect, as depicted in Figures 8a and 8b, diverging from observations in the Parguera Limestone (Figures 8 and 6, respectively).

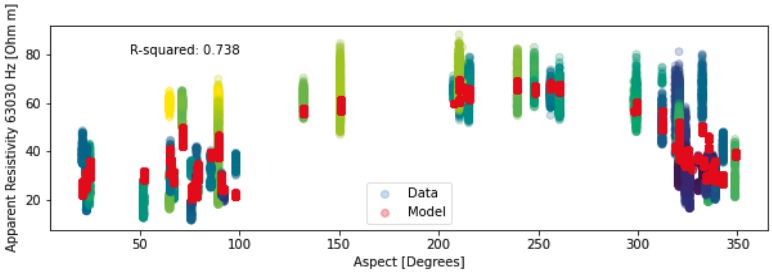


**Figure 9. Apparent resistivity with an OLS multivariate regression in Parguera Limestone based on all DEM parameters plotted against aspect.**

Figure 9 shows the 63030 Hz apparent resistivity with aspect and the results of an OLS regression model. The regression model incorporates elevation, aspect, slope, geographic position, and NDVI as parameters, resulting in an R-squared value of 0.779. Performing the OLS regression solely with aspect yields a lower R-squared value of 0.585 indicating aspect has a strong relationship to apparent resistivity but that other parameters such as elevation also have a substantial influence on the model.

While variations in mineralogy, porosity, clay content, and other factors may exist and are likely to cause some of the observed differences, it is probable that the observed localized differences in apparent resistivity primarily stem from moisture variations, akin to the earlier example seen in the Parguera Limestone. Factors such as microscale orographic effects, impacting precipitation patterns, or differential solar radiation across aspects, affecting moisture retention in the shallow subsurface, warrant further exploration. This topic requires additional

investigation but has implications for geotechnical and regional hazard analysis as subsurface materials may have different mechanical properties and weathering rates.

## CONCLUSIONS

Characterizing the subsurface across various scales in steep geologic environments is essential for accurate regional subsurface modeling and natural hazard risk assessment. This study demonstrates the capability of electromagnetic (EM) technology to create geospatial datasets that describe the shallow subsurface across scales, from meters to kilometers, providing an opportunity to integrate site-specific and regional estimates of subsurface variability. The spatial variation captured by the data offers valuable insights into influential topographic factors. EM's cost-effectiveness and scalability make it valuable for site-specific and regional hazard analysis. Further research is needed to validate and correlate EM data with traditional geotechnical tests.

This paper presents an innovative approach that employs handheld electromagnetic (EM) technology as a versatile and adaptable tool for investigating multiscale subsurface variability in geotechnical contexts. By merging and applying well-established methods to novel applications, the utilization of EM instruments is expanded. This integration underscores the tool's efficacy in advancing geotechnical engineering and illuminates new avenues for gaining a deeper understanding of subsurface dynamics and potential hazards.

## ACKNOWLEDGEMENTS

This study is financially supported by the NSF Frontier Research in Earth Science project under Grant No. 2021299 and 2020970 as well as by NASA through the Disasters program under grant No. 80NSSC20K1032 and 80NSSC19K0948. A special thanks to all members of the field reconnaissance team including Mirna Kassem, Dr. Stephen Hughes, Dr. Weibing Gong, and Dr. Stratis Karantanellis.

## REFERENCES

Allred, B. J., Daniels, J. J., and Ehsani, M. R. (2008). “Electromagnetic Induction Methods.” *Handbook of Agricultural Geophysics*, Daniels, J. J., Vendl, M., Ehsani, M. R., and Allred, J.J. CRC Press, (109–128).

Bawiec, W.J. (editor) (1998). "Geology, Geochemistry, Geophysics, Mineral Occurrences and Mineral Resource Assessment for the Commonwealth of Puerto Rico." *U.S. Geological Survey*. Open-File Report 98-38.

Donner, W., and H. Rodriguez. (2008). “Population Composition, Migration and Inequality: The Influence of Demographic Changes on Disaster Risk and Vulnerability.” *Social Forces,* 87(2), 1089–1114.

Doolittle, J. A., and Brevik, E. C. (2014). “The Use of Electromagnetic Induction Techniques in Soil Studies” *Geoderma*, 223-225, 33-45.

Finco, C., Rejiba, F., Schamper, C., Cavalcante Fraga, L.H., and Wang, A. (2023). “Calibration of near-surface multi-frequency electromagnetic induction data.” *Geophysical Prospecting*, 71, 765-779.

Godio, A., and G. Bottino. (2001). “Electrical and Electromagnetic Investigation for Landslide Characterisation.” *Physics and Chemistry of the Earth (C)*, 9, 705–710.

Hubbard, S. S., Schmutz, M., Balde, A., Falco, N., Peruzzo, L., Dafflon, B., Léger, E., and Wu, Y. (2021). "Estimation of Soil Classes and Their Relationship to Grapevine Vigor in a Bordeaux Vineyard: Advancing the Practical Joint Use of Electromagnetic Induction (EMI) and NDVI Datasets for Precision Viticulture." *Precision Agriculture*, 22(4), 1353-1376.

Huang, H. (2005). "Depth of investigation for small broadband electromagnetic sensors." *Geophysics*, 70(6).

McCann, D.M., and A. Forster. (1990). "Reconnaissance Geophysical Methods in Landslide Investigations." *Engineering Geology*, 29(1), 59–78.

Mohammed, M., El Mahmoudi, A., and Almolhem, Y. (2022). "Applications of Electromagnetic Induction and Electrical Resistivity Tomography for Digital Monitoring and Assessment of the Soil: A Case Study of Al-Ahsa Oasis, Saudi Arabia." *Applied Sciences*, 12(4).

Monroe, W. H. (1980) "Geology of the Middle Tertiary Formations of Puerto Rico." *U.S. Geological Survey*. Professional Paper 953.

Morales, A., Hughes, S., Lang, K., Rivera-Hernandez, F., Vargas, P., Lozano, J. M., Karantanellis, E., Kassem, M., Gomberg, D., Plescher, R., Irizarry, E., Vicens, E., Figueroa, T., Friedman, C., Cunillera, K., Ruiz, A., and Ortega, Victor. (2022). "Geotechnical Impacts of Hurricane Fiona in Puerto Rico". *Geotechnical Extreme Event Reconnaissance (GEER) Association*, GEER-081. Version 1. Online Publication.

Morales-Velez, A. C., Suarez L. E., Bernal J., Hughes K. S., Perez J. C., and Rodriguez, L. A. (2020). "2020 Puerto Rico Earthquake". *Geotechnical Extreme Event Reconnaissance (GEER) Association*, GEER-066. Version 1. Online Publication.

Triantafilis, J., and S.M. Lesch. (2005). "Mapping Clay Content Variation Using Electromagnetic Induction Techniques." *Computers and Electronics in Agriculture,* 46(1–3), 203–237.

Schmitt, R. G., Allstadt, K. E., Martinez, S. N., Bayouth Garcia, D., Hernandez, J., Schmitt, R. G., Perkins, J. P., Thompson, E. M., Hughes, S. K., Fuentes, Z., Brugman, E. I., Slaughter, S. L., and Grant, A. R. (2020). "Field Observations Of Ground Failure Triggered By the 2020 Puerto Rico earthquake sequence." *U.S. Geological Survey*. Data Set.

Silva-Tulla, F., Pando M. A., Soto A. E., Morales A., Pradel D., Inci G., Sasanakul I., Bernal J. R., Kayen R., Hughes S., Adams T., and Park Y. (2018). "2017 Hurricane Maria." *Geotechnical Extreme Event Reconnaissance (GEER) Association*, GEER-057, Version 1. Online Publication.

Smith, R. (2013). "Electromagnetic Induction Methods in Mining Geophysics from 2008 to 2012." *Surveys in Geophysics*, 35(1), 123–56.

USGS (U.S. Geological Survey), 2020, 3D Elevation Program 1/3 Arc-Second Resolution Digital Elevation Model (published 2020, 05, 05 and 2020, 05, 06), accessed February 2, 2023.

Won, I. J., Keiswetter, D. A., Fields, G. R. A., and Sutton, L. C. (1996). "GEM-2: A New Multifrequency Electromagnetic Sensor." *Journal of Environmental and Engineering Geophysics*, 1(2), 129–137.